



**Development of a
hydrostatic
dynamical core using
the CG/DG methods**

S.-J. Choi and
F. X. Giraldo

Development and evaluation of a hydrostatic dynamical core using the spectral element/discontinuous Galerkin methods

S.-J. Choi¹ and F. X. Giraldo²

¹Korea institute of atmospheric prediction systems, Seoul, Korea

²Naval Postgraduate School, Monterey, USA

Received: 23 May 2014 – Accepted: 17 June 2014 – Published: 26 June 2014

Correspondence to: S.-J. Choi (sj.choi@kiaps.org)

Published by Copernicus Publications on behalf of the European Geosciences Union.

Title Page

Abstract

Introduction

Conclusions

References

Tables

Figures

◀

▶

◀

▶

Back

Close

Full Screen / Esc

Printer-friendly Version

Interactive Discussion

Abstract

In this paper, we present a dynamical core for the atmospheric primitive hydrostatic equations using a unified formulation of spectral element (SE) and discontinuous Galerkin (DG) methods in the horizontal direction with a finite difference (FD) method in the radial direction. The CG and DG horizontal discretization employs high-order nodal basis functions associated with Lagrange polynomials based on Gauss–Lobatto–Legendre (GLL) quadrature points, which define the common machinery. The atmospheric primitive hydrostatic equations are solved on the cubed-sphere grid using the flux form governing equations in a three-dimensional (3-D) Cartesian space. By using Cartesian space, we can avoid the pole singularity problem due to spherical coordinates and this also allows us to use any quadrilateral-based grid naturally. In order to consider an easy way for coupling the dynamics with existing physics packages, we use a FD in the radial direction. The models are verified by conducting conventional benchmark test cases: the Rossby–Haurwitz wavenumber 4, Jablonowski–Williamson tests for balanced initial state and baroclinic instability, and Held–Suarez tests. The results from those tests demonstrate that the present dynamical core can produce numerical solutions of good quality comparable to other models.

1 Introduction

Spectral element (SE; here after is referred to as continuous Galerkin (CG)) and discontinuous Galerkin (DG) methods are very attractive on many-core computing platforms because these methods decompose the physical domain into smaller pieces having a small communication footprint. CG/DG methods are local in nature and thus can have a large on-processor operation count (Kelly and Giraldo, 2012) which is advantageous on large processor-count computers. Also CG/DG methods can achieve high-order accuracy because the polynomial order can be adjusted automatically according to the corresponding numerical integration rule, that is, the Gaussian

Development of a hydrostatic dynamical core using the CG/DG methods

S.-J. Choi and
F. X. Giraldo

Title Page

Abstract

Introduction

Conclusions

References

Tables

Figures

⏪

⏩

◀

▶

Back

Close

Full Screen / Esc

Printer-friendly Version

Interactive Discussion



quadrature (Taylor et al., 1997; Giraldo, 2001; Giraldo et al., 2002). In addition, CG/DG methods are geometrically flexible in the types of grids they can use; this includes static and adaptive grids as well as conforming and non-conforming grids (Giraldo et al., 2002; Giraldo and Rosmond, 2004; Mueller et al., 2013).

The CG method is characterized by the high-order approximation combined with the local decomposition property of the finite element method (FEM) and weak numerical dispersion property of the spectral method. The DG method, on the other hand, is best characterized as a combination of the properties of the CG method plus the local conservation properties of the finite volume method (FVM) (Giraldo and Restelli, 2008). The virtues of the DG method are that it is inherently conservative (both locally and globally) as in the case of the FVM. However, the common criticism of the DG method is the stringent Courant–Friedrichs–Lewy (CFL) stability constraint in explicit time schemes. For a DG method using k th order basis functions, an approximate CFL limit estimate is $1/(2k + 1)$ (Cockburn and Shu, 1989). This is partly due to the choice of the numerical flux which, for expediency, is chosen as a purely edge-based flux although other fluxes are also possible (e.g., Yelash et al., 2014); however these more sophisticated approaches come at a price and it is yet unclear which strategy yields a faster wallclock time to solution.

To date, successful applications of the CG method in hydrostatic atmospheric modeling include the Community Atmosphere Model – spectral element dynamical core (CAM-SE) (Dennis et al., 2012) and the scalable spectral element Eulerian atmospheric model (NSEAM) (Giraldo and Rosmond, 2004, hereafter GR04). In this context, one of the motivations of this study is to construct a dynamical core using a unified formulation of CG and DG methods as described in Giraldo and Restelli, 2008 and Kelly and Giraldo, 2012 where nonhydrostatic atmospheric models are proposed. Successful applications of the DG method in hydrostatic atmospheric modeling include the work of Nair et al., 2009; however, in our paper we shall present results for more than one test case. To our knowledge, the results for the Held–Suarez test cases presented in our paper are the first such results shown for a DG model. The significance is that

Development of a hydrostatic dynamical core using the CG/DG methods

S.-J. Choi and
F. X. Giraldo

Title Page

Abstract

Introduction

Conclusions

References

Tables

Figures

◀

▶

◀

▶

Back

Close

Full Screen / Esc

Printer-friendly Version

Interactive Discussion

Development of a hydrostatic dynamical core using the CG/DG methods

S.-J. Choi and
F. X. Giraldo

Title Page

Abstract

Introduction

Conclusions

References

Tables

Figures

◀

▶

◀

▶

Back

Close

Full Screen / Esc

Printer-friendly Version

Interactive Discussion

this confirms the long-term stability of the DG method for hydrostatic models. Although we could also discretize the vertical direction with CG and DG methods, we choose a conservative flux-form finite-difference method for discretization in the vertical direction which is similar to the approach used in both CAM-SE and NSEAM. This choice of vertical discretization provides an easy way for coupling the dynamics with existing physics packages.

In this paper we construct a unified formulation of CG and DG for the primitive hydrostatic equations in GR04. In order to achieve a unified formulation, the advective-form governing equations in GR04 are recast in flux form. GR04 provides a clue for converting the advective-form equation set in 3-D Cartesian space to the flux form in their appendix. By using 3-D Cartesian space, we can be free from the pole singularity problem in spherical coordinates. Although a local Cartesian coordinate system could also be used to overcome these problems (Taylor et al., 1997; Nair et al., 2005), the use of 3-D Cartesian space everywhere allows us to treat the pole as any other point. Therefore it permits general grids naturally such as icosahedral, hexahedral, and adaptive unstructured grids (it should be noted that general grids can also be used with the coordinate invariant form of the equations). In this paper we adopt a hexahedral grid – the so called cubed-sphere.

In brief, the objective of this paper is to show the feasibility of the hydrostatic primitive equation models using CG/DG horizontal discretization and the FD vertical discretization by conducting conventional benchmark test cases. The organization of the remainder of this paper is as follows. In the next section we describe the governing equations in 3-D Cartesian space with a definition of the prognostic and diagnostic variables. In Sect. 3 we explain the horizontal, vertical, and temporal discretization methods including the numerical approximation of the equations. In Sect. 4 we describe the cubed-sphere grid, and in Sect. 5, we present the simulation results of the test cases. Finally, in Sect. 6, we end the paper with a summary of our findings and some concluding remarks.

2 Governing equations

The primitive hydrostatic equations of conservation form in the 3-D Cartesian space with a sigma pressure vertical coordinate σ are given as

$$\frac{\partial \mathbf{q}}{\partial t} + \nabla \cdot \bar{\mathbf{F}} = \mathbf{S}_{\text{Cor}} + \mathbf{S}_h + \mathbf{S}_v, \quad (1)$$

5 where

$$\mathbf{q} = \begin{bmatrix} \pi \\ U \\ V \\ W \\ \Theta \end{bmatrix} = \begin{bmatrix} \pi \\ \pi U \\ \pi V \\ \pi W \\ \pi \theta \end{bmatrix} \quad (2)$$

are prognostic variables,

$$\mathbf{S}_{\text{Cor}} = \begin{bmatrix} 0 \\ -\frac{2\omega z}{a^2}(yW - zV) - \mu x \\ -\frac{2\omega z}{a^2}(zU - xW) - \mu y \\ -\frac{2\omega z}{a^2}(xV - yU) - \mu z \\ 0 \end{bmatrix}, \quad \mathbf{S}_h = \begin{bmatrix} 0 \\ (\varphi - \Theta c_p \frac{\partial P}{\partial \pi}) \frac{\partial \pi}{\partial x} \\ (\varphi - \Theta c_p \frac{\partial P}{\partial \pi}) \frac{\partial \pi}{\partial y} \\ (\varphi - \Theta c_p \frac{\partial P}{\partial \pi}) \frac{\partial \pi}{\partial z} \\ 0 \end{bmatrix}, \quad \mathbf{S}_v = \begin{bmatrix} -\frac{\partial}{\partial \sigma}(\pi \dot{\sigma}) \\ -\frac{\partial}{\partial \sigma}(U \dot{\sigma}) \\ -\frac{\partial}{\partial \sigma}(V \dot{\sigma}) \\ -\frac{\partial}{\partial \sigma}(W \dot{\sigma}) \\ -\frac{\partial}{\partial \sigma}(\Theta \dot{\sigma}) \end{bmatrix} \quad (3)$$

10 respectively denote Coriolis with the Lagrange multiplier μ , horizontal, and vertical source terms, and

$$\bar{\mathbf{F}} = \begin{bmatrix} \frac{U^2}{\pi} + \pi \varphi \\ \frac{VU}{\pi} \\ \frac{WU}{\pi} \\ \frac{\Theta U}{\pi} \end{bmatrix} \hat{i} + \begin{bmatrix} \frac{V^2}{\pi} + \pi \varphi \\ \frac{WV}{\pi} \\ \frac{\Theta V}{\pi} \end{bmatrix} \hat{j} + \begin{bmatrix} \frac{W^2}{\pi} + \pi \varphi \\ \frac{\Theta W}{\pi} \end{bmatrix} \hat{k} \quad (4)$$

4123

GMDD

7, 4119–4151, 2014

Development of a hydrostatic dynamical core using the CG/DG methods

S.-J. Choi and
F. X. Giraldo

Title Page

Abstract

Introduction

Conclusions

References

Tables

Figures

◀

▶

◀

▶

Back

Close

Full Screen / Esc

Printer-friendly Version

Interactive Discussion



is the horizontal flux terms where \hat{i} , \hat{j} , and \hat{k} denote the Cartesian directional unit vectors. The prognostic variables q are comprised of: (1) the surface pressure π defined as

$$\pi = p_s - p_t, \quad (5)$$

- 5 where p_s is the true surface pressure, and p_t is the pressure at the top of the atmosphere, (2) the flux-form velocity components $\mathbf{U} = (U, V, W) = (\pi u, \pi v, \pi w)$, where (u, v, w) are the three Cartesian velocity components, and (3) the flux-form potential temperature $\Theta = \pi\theta$, where θ is the potential temperature. The diagnostic variables are (1) the geopotential φ given by the diagnostic equation as

$$10 \quad \frac{\partial \varphi}{\partial P} = -c_p \theta, \quad (6)$$

(2) the Exner function P defined as

$$P = \left(\frac{p}{p_0} \right)^{R_d/c_p}, \quad (7)$$

- where p and p_0 is the hydrostatic pressure and standard surface pressure, respectively, and R_d and c_p is the gas constant and specific heat of dry air at constant pressure, and (3) the σ -coordinate vertical velocity $\dot{\sigma} = \frac{d\sigma}{dt}$ where $\sigma = \frac{p-p_t}{\pi} \in [0, 1]$ is the definition of the sigma pressure coordinate with a value of 0 at the top of the atmosphere and 1 at the surface. The constants a and ω in Eq. (3) are the Earth's radius and angular velocity, respectively, and μ is a Lagrange multiplier for the fluid particles to remain on a spherical shell with constant σ . The momentum variables representing the atmospheric motion over the shell in the Cartesian space have three components along the x , y , and z axes in Cartesian coordinates, so that the movement of a particle on the shell has three degrees of freedom, which can move freely in \mathbb{R}^3 . To ensure that fluid particles remain on the spherical shell, it is required that the fluid velocity remains

Development of a hydrostatic dynamical core using the CG/DG methods

S.-J. Choi and
F. X. Giraldo

Title Page

Abstract

Introduction

Conclusions

References

Tables

Figures

◀

▶

◀

▶

Back

Close

Full Screen / Esc

Printer-friendly Version

Interactive Discussion

Development of a hydrostatic dynamical core using the CG/DG methods

S.-J. Choi and
F. X. Giraldo

Title Page

Abstract

Introduction

Conclusions

References

Tables

Figures

◀

▶

◀

▶

Back

Close

Full Screen / Esc

Printer-friendly Version

Interactive Discussion

perpendicular to the position vector, which yields a Lagrange multiplier in the momentum equations (Giraldo, 2001; Giraldo et al., 2002; Giraldo and Rosmond, 2004). It is noteworthy that among the independent variables (x, y, z, σ, t) , (x, y, z) represent grid points on the sphere which are related to the points in the spherical coordinates (λ, ϕ) given as

$$\begin{aligned}x &= a \cos \lambda \cos \phi, \\y &= a \sin \lambda \cos \phi, \\z &= a \sin \phi.\end{aligned}\tag{8}$$

Thus ∇ is defined as

$$\nabla = \begin{pmatrix} \frac{\partial}{\partial x} \\ \frac{\partial}{\partial y} \\ \frac{\partial}{\partial z} \end{pmatrix}\tag{9}$$

at constant σ .

3 Discretization

3.1 Discretization in the horizontal direction

To describe the discretization of the horizontal operators by the CG/DG method we follow the description given previously in Giraldo and Restelli, 2008 and in Kelly and Giraldo, 2012. Let us begin by rewriting Eq. (1) as follows

$$\frac{\partial q}{\partial t} + \nabla \cdot \mathbf{F} = S\tag{10}$$

Next, let us introduce the following vector spaces

$$V^{\text{CG}} = \left\{ \psi \in H^1(\Omega) \mid \psi \in P_N(\Omega_e) \right\}\tag{11}$$

and

$$V^{\text{DG}} = \left\{ \psi \in L^2(\Omega) \mid \psi \in P_N(\Omega_e) \right\} \quad (12)$$

where we now seek solutions of Eq. (1) as follows:

$$q \in V \quad \forall \psi \in V$$

5 where V denotes either V^{CG} or V^{DG} . Next, we approximate the solution vector as follows

$$\mathbf{q}_N(x, y, z, t) = \sum_{i=1}^M \psi_i(x, y, z) q_i(t) \quad (13)$$

where, for quadrilateral elements in the horizontal direction, $M = (N + 1)^2$ with N representing the polynomial order of the basis function ψ .

10 We now introduce this expansion into our governing system of equations, multiply by a test function, and integrate by parts to yield

$$\int_{\Omega_e} \psi_i \frac{\partial \mathbf{q}_N}{\partial t} d\Omega_e + \int_{\Gamma_e} \psi_i \hat{n} \cdot \mathbf{F} d\Gamma_e - \int_{\Omega_e} \nabla \psi_i \cdot \mathbf{F}(\mathbf{q}_N) d\Omega_e = \int_{\Omega_e} \psi_i S(\mathbf{q}_N) d\Omega_e. \quad (14)$$

where the terms with Ω_e refer to volume integrals and the one with Γ_e is a boundary integral which accounts for internal faces (neighboring elements share faces). In
15 matrix-vector form, this equation can be written as

$$\mathbf{M}_{i,j}^e \frac{dq_j^e}{dt} + \left(\mathbf{M}_{i,j}^{\text{F},e} \right)^T \cdot \mathbf{F}_j^*(\mathbf{q}_N) - \left(\tilde{\mathbf{D}}_{i,j}^e \right)^T \cdot \mathbf{F}_j(\mathbf{q}_N^e) = \mathbf{M}_{i,j}^e S_j(\mathbf{q}_N^e) \quad (15)$$

where

$$\begin{aligned}\mathbf{M}_{i,j}^e &= \int_{\Omega_e} \psi_i \psi_j d\Omega_e, \\ \mathbf{M}_{i,j}^{F,e} &= \int_{\Gamma_e} \psi_i \psi_j \hat{n} d\Gamma_e, \\ \tilde{\mathbf{D}}_{i,j}^e &= \int_{\Omega_e} \nabla \psi_i \psi_j d\Omega_e.\end{aligned}\tag{16}$$

These matrices represent: the mass, flux, and differentiation matrices, respectively.

For the DG method, the matrix-vector form given above is sufficient as long as we define the numerical flux, e.g., as follows

$$F^*(q_N) = \frac{1}{2} \left[F(q_N^L) + F(q_N^R) - \hat{n} |\lambda_{\max}| (q_N^R - q_N^L) \right]\tag{17}$$

where the superscripts L and R refer to the left and right elements (arbitrarily decided) of the face Γ_e and λ_{\max} is the maximum eigenvalue of the Jacobian matrix of the governing partial differential equations. Here we use the Rusanov scheme for the numerical flux because of its simplicity although any other Riemann solver could be used. For the CG method, the matrix-vector form given above is also used except that the term of the flux matrix vanishes on the sphere and we then use the direct stiffness summation (DSS) operation which gathers the element-wise solution to a global grid point solution and then scatters it back to the element-wise space. This is done to ensure that the solution is C^0 across all element faces.

3.2 Discretization in the vertical direction

We use the FD method similarly to other global models to gain an easy way for coupling the dynamics with existing physics packages, although we could also discretize the

GMDD

7, 4119–4151, 2014

Development of a hydrostatic dynamical core using the CG/DG methods

S.-J. Choi and
F. X. Giraldo

Title Page

Abstract

Introduction

Conclusions

References

Tables

Figures

◀

▶

◀

▶

Back

Close

Full Screen / Esc

Printer-friendly Version

Interactive Discussion



vertical operators with the CG/DG methods (as done in Kelly and Giraldo, 2012; Giraldo et al., 2013). Also by using the FD, we can keep the model as similar as possible to the NSEAM model (GR04) so that we directly discern differences from the discrete horizontal operators. Using a Lorenz staggering, the variables U , V , W , Θ , and φ are at layer mid points denoted by $k = 1, 2, \dots, N_{\text{lev}}$ where N_{lev} is the total number of layers, while the variable P and $\dot{\sigma}$ are at layer interface points denoted by $k + \frac{1}{2}$, $k = 0, 1, \dots, N_{\text{lev}}$.

We begin the vertical discretization by the evaluating $\frac{\partial \pi}{\partial t}$ which is given by integrating the first row of Eq. (1) (i.e., the continuity equation) from the surface ($\sigma_{\text{bottom}} = \sigma_{N_{\text{lev}}+1/2} = 1$) to the top ($\sigma_{\text{top}} = \sigma_{1/2} = 0$) with no-flux boundaries at the top and bottom levels of the atmosphere (i.e. $\dot{\sigma}_{\text{top}} = \dot{\sigma}_{\text{bottom}} = 0$). Thus,

$$\frac{\partial \pi}{\partial t} = \mathbf{M}^{-1} \sum_{k=1}^{N_{\text{lev}}} \tilde{\mathbf{D}} \cdot \mathbf{U}_k \Delta \sigma_k, \quad (18)$$

where k is the number of vertical levels to be integrated across and $\Delta \sigma_l = \sigma_{l+1/2} - \sigma_{l-1/2}$ is the thickness of the layer. Then the vertical velocity $\dot{\sigma}$ at each vertical level is obtained by integrating the continuity equation from the top of the atmosphere to the material surface as follows

$$(\dot{\sigma})_{k+1/2} = -\frac{\partial \pi}{\partial t} \sigma_{k+1/2} + \mathbf{M}^{-1} \sum_{l=1}^k \tilde{\mathbf{D}} \cdot \mathbf{U}_l \Delta \sigma_l. \quad (19)$$

The vertical advection term $\frac{\partial(\dot{\sigma}q)}{\partial \sigma}$ in the vertical source term \mathbf{S}_v is computed using the third-order upwind biased discretization in Hundsdoerfer et al. (1995) which is given as

$$\left. \frac{\partial f}{\partial \sigma} \right|_k = \frac{f_{k-2} - 8f_{k-1} + 8f_{k+1} - f_{k+2}}{12\Delta\sigma} + \text{sign}(\dot{\sigma}) \frac{f_{k-2} - 4f_{k-1} + 6f_k - 4f_{k+1} + f_{k+2}}{12\Delta\sigma}, \quad (20)$$

where f denotes the flux ($\dot{\sigma}q$). It is noted that the upwind-biased schemes are inherently diffusive. Following GR04, the hydrostatic equation, Eq. (6), is evaluated as

GMDD

7, 4119–4151, 2014

Development of a hydrostatic dynamical core using the CG/DG methods

S.-J. Choi and
F. X. Giraldo

Title Page

Abstract

Introduction

Conclusions

References

Tables

Figures

◀

▶

◀

▶

Back

Close

Full Screen / Esc

Printer-friendly Version

Interactive Discussion



follows

$$\varphi_k - \varphi_{k+1} = c_p \Theta_k (P_{k+1/2} - P_k) + c_p \Theta_{k+1} (P_{k+1} - P_{k+1/2}), \quad (21)$$

where the Exner function at layer interfaces and midpoints is given by

$$P_{k+1/2} = \left(\frac{p_{k+1/2}}{p_0} \right)^\kappa \quad (22)$$

5 and

$$P_k = \frac{1}{\kappa + 1} \frac{1}{p_0^\kappa} \left(\frac{p_{k+1/2}^{\kappa+1} - p_{k-1/2}^{\kappa+1}}{p_{k+1/2} - p_{k-1/2}} \right), \quad (23)$$

respectively.

3.3 Discretization in time

10 For integrating the equations, we adopt a third-order strong stability preserving explicit Runge–Kutta (SSP-RK) scheme (Cockburn and Shu, 1998; Nair et al., 2005). The 3rd order SSP-RK scheme is introduced into our governing equations in the form of

$$\frac{\partial q}{\partial t} = R(q), \quad (24)$$

and is given as follows:

$$\begin{aligned} q^{(1)} &= q^n + \Delta t R(q^n) \\ 15 \quad q^{(2)} &= \frac{3}{4} q^n + \frac{1}{4} q^{(1)} + \frac{1}{4} \Delta t R(q^{(1)}) \\ q^{n+1} &= \frac{1}{3} q^n + \frac{2}{3} q^{(1)} + \frac{2}{3} \Delta t R(q^{(2)}), \end{aligned} \quad (25)$$

**Development of a
hydrostatic
dynamical core using
the CG/DG methods**

S.-J. Choi and
F. X. Giraldo

Title Page

Abstract

Introduction

Conclusions

References

Tables

Figures

◀

▶

◀

▶

Back

Close

Full Screen / Esc

Printer-friendly Version

Interactive Discussion



where the superscripts n and $n + 1$ denote time levels t and $t + \Delta t$, respectively. While for smooth problems the SSP-RK scheme does not generate spurious oscillations so that are widely used for DG methods, for problems with strong shocks or discontinuities, oscillations can lead to nonlinear instabilities (Cockburn and Shu, 1998). Since an SSP-RK time-integration scheme cannot control such undesirable effects, a Boyd–Vandeven spatial filter is applied after the time integration, which is described in GR04. Neither viscosity nor slope limiter are used in all simulations.

4 Cubed-sphere grid

The cubed-sphere grids are composed of the six patches obtained by the gnomonic projection of the faces of the hexahedron which are subdivided into $(n_H \times n_H)$ quadrilateral elements where n_H is the number of quadrilateral elements in each direction (GR04). Inside each element we build $(N + 1)$ Gauss–Lobatto–Legendre (GLL) quadrature points, where N indicate the polynomial order of the basis function ψ . Therefore the total number of grid points N_p is given as

$$N_p = 6(n_H N)^2 + 2, \quad (26)$$

and the number of elements N_e comprising the sphere is

$$N_e = 6(n_H)^2. \quad (27)$$

We now introduce the square region on the gnomonic space $(\xi_G, \eta_G) = [-\frac{\pi}{4}, +\frac{\pi}{4}]^2$ in each of the six faces to describe the relation to spherical coordinates (λ, ϕ) . The gnomonic space $(\xi_G, \eta_G) = [-\frac{\pi}{4}, +\frac{\pi}{4}]^2$ is mapped to the corresponding spherical co-

5.1 3-D Rossby–Haurwitz wavenumber 4

We conduct the Rossby–Haurwitz (RH) wave test case which is a 3-D extension of the 2-D shallow water RH wave discussed in Williamson et al. (1992). The main differences compared to the 2-D shallow water formulation include the introduction of a temperature field and the derivation of the surface pressure, which is discussed in GR04 and Jablonowski et al. (2008). The Rossby–Haurwitz wave approximately preserves its shape even in nonlinear shallow water and primitive equation models, which has a sufficiently simple enough pattern to allow one to judge if the simulation was successful. We initialize the model following Jablonowski et al. (2008).

Snapshots of the output data for the CG and DG models for day 15 are presented in Figs. 2 and 3, respectively. The figures show the 850 hPa zonal wind, meridional wind, and temperature as well as the surface pressure. These model results were computed at the resolution of $H = 64$ ($n_H = 8$ and $N = 8$) with 26 vertical levels ($N_{lev} = 26$). The results of the CG and DG simulations are virtually indistinguishable; in addition, the accuracy results of both simulations are almost identical to the results obtained with the CAM3.5.41 version of the NCAR Finite Volume (FV) dynamical core at the resolution 1° by 1° with 26 hybrid levels, as described in Jablonowski et al. (2008). Although we have used a relatively low resolution of H64 which is comparable to T63 of a spectral model, the results are strikingly similar to the solutions with the $1^\circ \times 1^\circ$ NCAR CAM-FV core, both in phase and amplitude.

5.2 Jablonowski–Williamson balanced initial state test

In order to estimate the accuracy and stability of the dynamical core, we conduct the Jablonowski–Williamson balanced initial state test introduced by Jablonowski and Williamson (2006). We initialize the model following Jablonowski and Williamson (2006). Using the balanced initial fields, the simulation results should maintain the initial state perfectly for a sufficient amount of time. Since the initial state of this test is the true solution, we can compute error norms. We evaluate the error by using the relative

Development of a hydrostatic dynamical core using the CG/DG methods

S.-J. Choi and F. X. Giraldo

Title Page

Abstract

Introduction

Conclusions

References

Tables

Figures

◀

▶

◀

▶

Back

Close

Full Screen / Esc

Printer-friendly Version

Interactive Discussion



L_2 error defined by

$$\|q_{\text{simulation}}\|_{L_2} = \sqrt{\frac{\int_{\Omega} (q_{\text{exact}} - q_{\text{simulation}})^2 d\Omega}{\int_{\Omega} q_{\text{exact}}^2 d\Omega}},$$

where $q_{\text{simulation}}$ represents the computed state variables and q_{exact} the exact (i.e., initial condition) values.

Figure 4 shows the normalized surface pressure L_2 error norms for the CG and DG simulations with $H = 128$ ($n_H = 16$ and $N = 8$) horizontal resolution and 26 vertical levels ($N_{\text{lev}} = 26$). The L_2 error norms of the two simulations are visually identical, in which the error oscillates but remains bounded. These results (including the value of the L_2 error) compare well against those of the NSEAM model presented in GR04. The bounded error confirms that the initial balanced state is properly maintained. In practice though, the initial state degrades over time. After 20 days, the zonal wind fields for the CG and DG simulations show a somewhat distorted distribution with an increasing zonally asymmetric pattern (Fig. 5). Initially the maximum of the zonal winds at the lowest level are about 9.4 m s^{-1} in mid-latitude, but after 20 days the maximum difference of the zonal wind is up to about 0.02 m s^{-1} showing the zonal asymmetry. Although the error distribution is different between the CG and DG simulations in detail, these have a wavenumber 4 structure which arise from the cubed-sphere grid. The wavenumber 4 signals grow over time and lead eventually to a breakdown of the balanced state. However, higher resolutions delay the growth of the signals as the truncation error associated with the spatial discretization decreases. Actually, at $H = 192$ ($n_H = 16$ and $N = 12$) horizontal resolution this error virtually disappears for 20 day simulations (Fig. 6).

5.3 Jablonowski–Williamson baroclinic instability test

The baroclinic instability test case starts from the balanced initial fields, which is described above, with a perturbation in the initial zonal velocity. The baroclinic wave is

GMDD

7, 4119–4151, 2014

Development of a hydrostatic dynamical core using the CG/DG methods

S.-J. Choi and
F. X. Giraldo

Title Page

Abstract

Introduction

Conclusions

References

Tables

Figures

◀

▶

◀

▶

Back

Close

Full Screen / Esc

Printer-friendly Version

Interactive Discussion



induced by the small perturbation in the initial zonal wind. Here a Gaussian profile is used for the zonal wind perturbation, which is centered at $(\lambda_c, \phi_c) = (\frac{\pi}{9}, \frac{2\pi}{9})$ pointing to the location (20° E, 40° N). This perturbation is given by

$$u_{\text{perturbation}}(\lambda, \phi, \sigma) = \exp \left[- \left(\frac{r}{R} \right)^2 \right],$$

where

$$r = a \arccos [\sin \phi_c \sin \phi + \cos \phi_c \cos \phi \cos(\lambda - \lambda_c)],$$

and $R = a/10$ is the perturbation radius (Jablonowski and Williamson, 2006).

Since the baroclinic wave test case does not have an analytic solution, we compare our results to the solutions from Jablonowski and Williamson (2006) and the NSEAM model in GR04. We show the surface pressure, 850 hPa temperature, and 850 hPa relative vorticity at day 9 for the CG and DG simulations with the resolution of $H = 80$ ($n_H = 16$ and $N = 5$) and 26 vertical levels ($N_{\text{lev}} = 26$) in Fig. 7 which can be compared with the solutions of the National Center for Atmospheric Research's Community Atmosphere Model version 3 (NCAR CAM3) Eulerian dynamical core at T85 resolution and finite volume core at 1° by 1.25° from Jablonowski and Williamson (2006).

The CG and DG simulations in Fig. 7 are visually very similar to those reported in Jablonowski and Williamson with regard to the structure in the fields and the extrema for the surface pressure; in addition, the CG and DG results are almost identical to each other. Differences, however, can only be seen in the relative vorticity field at very small scales. In the CG simulation, the small-scale vorticity in the vicinity of the hook is depicted, and the maximum strength of the relative vorticity is larger than that of the DG simulation, which can be also seen in the results of a relatively higher resolution shown in Fig. 8. Figure 8 shows the same fields at day 9 as in Fig. 7 but for the higher resolution of $H = 160$ ($n_H = 32$ and $N = 5$) and 26 vertical levels ($N_{\text{lev}} = 26$). In comparison with the results of the lower resolution of $H = 80$ ($n_H = 16$ and $N = 5$), it can be clearly seen that the numerical solutions of the two different resolutions are well converged in terms

Development of a hydrostatic dynamical core using the CG/DG methods

S.-J. Choi and
F. X. Giraldo

Title Page

Abstract

Introduction

Conclusions

References

Tables

Figures

◀

▶

◀

▶

Back

Close

Full Screen / Esc

Printer-friendly Version

Interactive Discussion



Development of a hydrostatic dynamical core using the CG/DG methods

S.-J. Choi and
F. X. Giraldo

Title Page

Abstract

Introduction

Conclusions

References

Tables

Figures

◀

▶

◀

▶

Back

Close

Full Screen / Esc

Printer-friendly Version

Interactive Discussion



of the strength and structure in the surface pressure, temperature, and vorticity fields. It is noted that the vorticity fields in the higher resolution are characterized by the smallest scale in the vicinity of the hook, which is the same as in the lower resolution, which imply that the DG simulation is more diffusive than the CG simulation. It suggests that the diffusive property of the DG simulation is induced by the Rusanov numerical flux used in this study, because the only difference between the CG and DG formulations is the numerical flux and the fact that the DG solutions are allowed to contain jumps across element edges. However, this difference in the results suggests that it is the dissipation of the numerical flux that is mainly responsible for the differences in the two simulations.

In general, the baroclinic wave grows observably around day 4. At day 7 the baroclinic wave evolves rapidly and by day 9 the wave train has intensified significantly (Jablonowski and Williamson, 2006). In order to examine the growth of the perturbation, an evolution of the minimum surface pressure is shown in Fig. 9 which we now compare with the results in GR04. The results of the CG and DG simulations with different resolutions are almost in agreement until day 10, at which point the simulations begin to show slight deviations from each other. The DG simulation with the lower resolution tends to simulate somewhat weak deepening. During the period between day 10 and 11 when wave breaking has set in, the remarkable weak deepening is shown in the DG simulation at the lower resolution. At day 14, the difference of the minimum surface pressure between the DG simulation at the lower resolution and the three other simulations is about 2 hPa.

5.4 Held–Suarez test

In order to estimate the capabilities of the model in simulating a realistic climate circulation without complex parameterizations, we conduct the Held–Suarez test. The Held–Suarez test ensures that a dynamical core produces a realistic zonal and time mean climate and synoptic eddies by using a simple Newtonian relaxation of the temperature field and a Rayleigh damping of low-level winds representing boundary-layer

friction (Held and Suarez, 1994). The Newtonian relaxation of the temperature is added as the diabatic forcing term to the thermodynamic equation, the fifth row of Eq. (1), and the Rayleigh damping is imposed as dissipation term in the momentum equation, the second to fourth rows of Eq. (1). The detailed specifications are adapted from Held and Suarez (1994). For this test we use a relatively low resolution of $H = 40$ ($n_H = 8$ and $N = 5$) with 25 vertical levels ($N_{lev} = 25$) because this test case requires a relatively long model time simulation for 1200 days. In this paper, the integrations start from a stably stratified state at rest atmosphere, in which the lapse rate of temperature is 6.5 K m^{-1} and the surface temperature is 288 K. We use the simulation results from day 200 to day 1200 integrations sampled every 10 days.

Figure 10 shows the time mean zonally averaged zonal wind and temperature for both the CG and DG simulations which can be easily compared to the results of other published papers. In comparison with the results of the spectral transform model in Held and Suarez (1994), both the CG and DG simulations show reasonable and comparable distributions, where the midlatitude jets at the upper troposphere near 250 hPa and the equatorial easterly flow in the lower and upper atmosphere are clearly visible in each hemisphere. Also temperature stratification is maintained realistically. The simulation results are comparable to that of GR04. There exist, however, differences between the results of the CG and DG simulations mainly in the strength of the westerly flow and the temperature structure in the upper atmosphere. DG simulates broader upper-level jet streams than CG that strengthen with altitude. Also in the temperature field, the DG simulation shows warmer air in the equatorial upper atmosphere. The difference is shown clearly in Fig. 11 where we plot the time mean zonally averaged eddy heat flux of the CG and DG simulations. There are two maxima at mid-latitude in the lower and upper atmosphere indicating transportations of heat in the poleward direction, of which the distributions in the CG and DG simulations are in good agreement with previous studies, for example, Held and Suarez (1994), Lin (2004) and Wan et al. (2008). However, in comparison of the strength and horizontal gradient of the eddy heat flux between both simulations, CG simulates a stronger eddy motion than DG.

Development of a hydrostatic dynamical core using the CG/DG methods

S.-J. Choi and
F. X. Giraldo

[Title Page](#)
[Abstract](#)
[Introduction](#)
[Conclusions](#)
[References](#)
[Tables](#)
[Figures](#)
[◀](#)
[▶](#)
[◀](#)
[▶](#)
[Back](#)
[Close](#)
[Full Screen / Esc](#)
[Printer-friendly Version](#)
[Interactive Discussion](#)


6 Summary and conclusions

We have proposed a hydrostatic dynamical solver using both the continuous Galerkin (CG) and discontinuous Galerkin (DG) methods. It is solved on a cubed-sphere grid in 3-D Cartesian coordinates although in principle any quadrilateral-based grid could be used. The CG and DG horizontal discretization employs a high-order nodal (Lagrange) basis function based on quadrilateral elements and GLL quadrature points which compose the common machinery. However, the DG method use fluxes along the boundaries of the elements which are approximated by the Rusanov method. In the vertical direction, a conservative flux-form finite-difference method is employed for coupling the dynamics with existing physics packages easily; we hope to report progresses on this specific topic in the future. A third-order strong stability preserving Runge–Kutta scheme was used for time integration although other time-integrators (including semi-implicit methods) could also be used.

In this paper, we show simulations of the model using four baroclinic test cases including: the Rossby–Haurwitz wave, balanced initial state, baroclinic instability, and Held–Suarez test cases. All cases, except for the Jablonowski–Williamson balanced initial state test case, do not have analytic solutions. Therefore, we compare our results to the results of test cases run by a vast community. Through our comparison of the CG and DG simulations, we show that for the baroclinic instability test and Held–Suarez test cases, the DG simulation tends to simulate somewhat weaker small-scale features, such as the minimum surface pressure perturbation and eddy heat flux, than the CG method. This could be due to the intrinsic diffusion of the Rusanov numerical flux scheme used for the horizontal discretization of the DG method, which is the only difference between the CG and DG formulations. One of the valuable contributions of this model is that we can use it to study the effects of using different horizontal discretizations since we use the exact same model with the same finite difference method in the vertical and time-integration methods but use either CG or DG in the horizontal. The discrete operators in the horizontal use the exact same numerical machinery

Development of a hydrostatic dynamical core using the CG/DG methods

S.-J. Choi and
F. X. Giraldo

Title Page

Abstract

Introduction

Conclusions

References

Tables

Figures

◀

▶

◀

▶

Back

Close

Full Screen / Esc

Printer-friendly Version

Interactive Discussion



Development of a hydrostatic dynamical core using the CG/DG methods

S.-J. Choi and
F. X. Giraldo

Title Page

Abstract

Introduction

Conclusions

References

Tables

Figures

◀

▶

◀

▶

Back

Close

Full Screen / Esc

Printer-friendly Version

Interactive Discussion

and so the results shown here isolate the differences offered by the CG and DG methods. However, for the other two test cases (Rossby–Haurwitz wave and balanced initial state tests), the results of the CG and DG simulations are virtually indistinguishable. Furthermore, the numerical results obtained for all four test cases show that the present dynamical core can produce numerical solutions of good quality comparable to other models. The results confirm that the CG and DG methods combined with the finite difference method in the vertical direction offer a viable strategy for atmospheric modeling. To our knowledge, we present the first results for a DG model for long-time simulations represented by the Held–Suarez test case. The importance of this result is that this confirms the stability of the DG method for long-time simulations in hydrostatic atmospheric dynamics. In order to make the model efficient and competitive with operational models, we need a semi-implicit time integration method which, although requires some additional machinery to be added, does not pose any theoretical barriers since such algorithms have already been designed by one of the authors in previous papers (Giraldo, 2005; Giraldo et al., 2013).

Based on the implementation of the horizontally CG/DG vertically finite difference method for the global hydrostatic dynamical core in this study, further research will focus on developing a global non-hydrostatic dynamical core. As an initial effort, we have investigated feasibilities of the combined spatial discretization method of the horizontally CG and vertically finite difference method for the development of a non-hydrostatic dynamical core in a two dimensional framework (Choi et al., 2014).

Acknowledgements. This work has been carried out through the R&D project on the development of global numerical weather prediction systems of Korea Institute of Atmospheric Prediction Systems (KIAPS) funded by Korea Meteorological Administration (KMA). The first author is grateful for the MA4245 course (taught by F. X. Giraldo) which laid out the framework for the unified CG/DG approach. The second author gratefully acknowledges the support of KIAPS, the Office of Naval Research through program element PE-0602435N and the National Science Foundation (Division of Mathematical Sciences) through program element 121670.

References

- Choi, S.-J., Giraldo, F. X., Kim, J., and Shin, S.: Verification of a non-hydrostatic dynamical core using horizontally spectral element vertically finite difference method: 2-D aspects, *Geosci. Model Dev. Discuss.*, 7, 3717–3750, doi:10.5194/gmdd-7-3717-2014, 2014.
- 5 Cockburn, B. and Shu, C.: The Runge–Kutta discontinuous Galerkin finite element method for conservation laws. V: Multidimensional systems, *J. Comput. Phys.*, 141, 199–224, 1998.
- Dennis, J. M., Edwards, J., Evans, K. J., Guba, O., Lauritzen, P. H., Mirin, A. A., St-Cyr, A., Taylor, M. A., and Worley, P. H.: CAM-SE: a scalable spectral element dynamical core for the Community Atmosphere Model, *Int. J. High Perform. C.*, 26, 74–89, 2012.
- 10 Giraldo, F. X.: A spectral element shallow water model on spherical geodesic grids, *Int. J. Numer. Method. H.*, 35, 869–901, 2001.
- Giraldo, F. X.: Semi-implicit time-integrators for a scalable spectral element atmospheric model, *Q. J. Roy. Meteor. Soc.*, 131, 2431–2454, 2005.
- Giraldo, F. X. and Restelli, M.: A study of spectral element and discontinuous Galerkin methods for the Navier–Stokes equations in nonhydrostatic mesoscale atmospheric modeling: equation sets and test cases, *J. Comput. Phys.*, 227, 3849–3877, 2008.
- 15 Giraldo, F. X. and Rosmond, T. E.: A Scalable Spectral Element Eulerian Atmospheric Model (SEE-AM) for NWP: dynamical core tests, *Mon. Weather Rev.*, 132, 133–153, 2004.
- Giraldo, F. X., Hesthaven, J. S., and Warburton, T.: Nodal high-order discontinuous Galerkin methods for the spherical shallow water equations, *J. Comput. Phys.*, 181, 499–525, 2002.
- 20 Giraldo, F. X., Kelly, J. F., and Constantinescu, E. M.: Implicit–explicit formulations for a 3D Nonhydrostatic Unified Model of the Atmosphere (NUMA), *SIAM J. Sci. Comput.*, 35, B1162–B1194, 2013.
- Held, I. M. and Suarez, M. J.: A proposal for the intercomparison of the dynamical cores of atmospheric general circulation models, *B. Am. Meteorol. Soc.*, 75, 1825–1830, 1994.
- 25 Hundsdoerfer, W., Koren, B., van Loon, M., and Verwer, K. G.: A positive finite-difference advection scheme, *J. Comput. Phys.*, 117, 35–46, 1995.
- Jablonowski, C. and Williamson, D. L.: A baroclinic instability test case for atmospheric model dynamical cores, *Q. J. Roy. Meteor. Soc.*, 132, 2943–2975, 2006.
- 30 Jablonowski, C., Lauritzen, P., Nair, R., and Taylor, M.: Idealized test cases for the dynamical cores of atmospheric general circulation models: a proposal for the ncar asp 2008 summer colloquium, Manuscript May/29/2008, NCAR Technical Report and Journal Paper, avail-

Development of a hydrostatic dynamical core using the CG/DG methods

S.-J. Choi and
F. X. Giraldo

Title Page

Abstract

Introduction

Conclusions

References

Tables

Figures

◀

▶

◀

▶

Back

Close

Full Screen / Esc

Printer-friendly Version

Interactive Discussion



able at: http://www-personal.umich.edu/~cjablono/dycore_test_suite.html#dynamical_core_tests, submitted, 2008.

Kelly, J. F. and Giraldo, F. X.: Continuous and discontinuous Galerkin methods for a scalable three-dimensional nonhydrostatic atmospheric model: limited-area mode, *J. Comput. Phys.*, 231, 7988–8008, 2012.

Lin, S.-J.: A “vertically Lagrangian” finite-volume dynamical core for global models, *Mon. Weather Rev.*, 132, 2293–2307, 2004.

Müller, A., Behrens, J., Giraldo, F. X., and Wirth, V.: Comparison between adaptive and uniform discontinuous Galerkin simulations in dry 2D bubble experiments, *J. Comput. Phys.*, 235, 371–393, 2013.

Nair, R. D., Thomas, S. J., and Loft, R. D.: A discontinuous Galerkin global shallow water model, *Mon. Weather Rev.*, 133, 876–888, 2005.

Nair, R. D., Choi, H.-W., and Tufo, H. M.: Computational aspects of a scalable high-order discontinuous Galerkin atmospheric dynamical core, *Comput. Fluids*, 38, 309–319, 2009.

Taylor, M., Tribbia, J., and Iskandarani, M.: The spectral element method for the shallow water equations on the sphere, *J. Comput. Phys.*, 130, 92–108, 1997.

Wan, H., Giorgetta, M. A., and Bonaventura, L.: Ensemble Held–Suarez test with a spectral transform model: variability, sensitivity, and convergence, *Mon. Weather Rev.*, 136, 1075–1092, 2008.

Williamson, D. L., Drake, J. B., Hack, J., Jacob, R., and Swartztrauber, P. N.: A standard test set for numerical approximations to the shallow water equations in spherical geometry, *J. Comput. Phys.*, 102, 211–224, 1992.

Yelash, L., Muller, A., Lukacova-Medvidova, M., Giraldo, F. X., and Wirth, V.: Adaptive discontinuous evolution Galerkin method for dry atmospheric flow, *J. Comput. Phys.*, 268, 106–133, 2014.

GMDD

7, 4119–4151, 2014

Development of a hydrostatic dynamical core using the CG/DG methods

S.-J. Choi and
F. X. Giraldo

Title Page

Abstract

Introduction

Conclusions

References

Tables

Figures

◀

▶

◀

▶

Back

Close

Full Screen / Esc

Printer-friendly Version

Interactive Discussion

Development of a hydrostatic dynamical core using the CG/DG methods

S.-J. Choi and
F. X. Giraldo

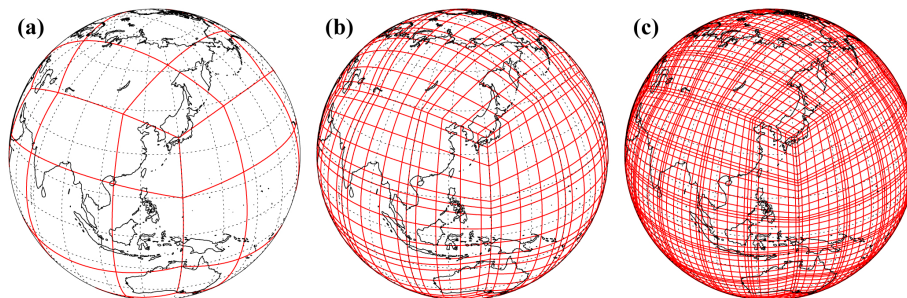


Figure 1. The cubed-sphere grid for **(a)** the $H = 3$ ($n_H = 3$ and $N = 1$), **(b)** the $H = 15$ ($n_H = 3$ and $N = 5$), and **(c)** the $H = 35$ ($n_H = 5$ and $N = 7$) horizontal resolutions.

[Title Page](#)[Abstract](#)[Introduction](#)[Conclusions](#)[References](#)[Tables](#)[Figures](#)[I ◀](#)[▶ I](#)[◀](#)[▶](#)[Back](#)[Close](#)[Full Screen / Esc](#)[Printer-friendly Version](#)[Interactive Discussion](#)

Development of a hydrostatic dynamical core using the CG/DG methods

S.-J. Choi and
F. X. Giraldo

Title Page

Abstract

Introduction

Conclusions

References

Tables

Figures

◀

▶

◀

▶

Back

Close

Full Screen / Esc

Printer-friendly Version

Interactive Discussion

Snapshots of the Rossby-Haurwitz wave at day 15
simulated with KIAPS-H_CG.Np08xNe08L26

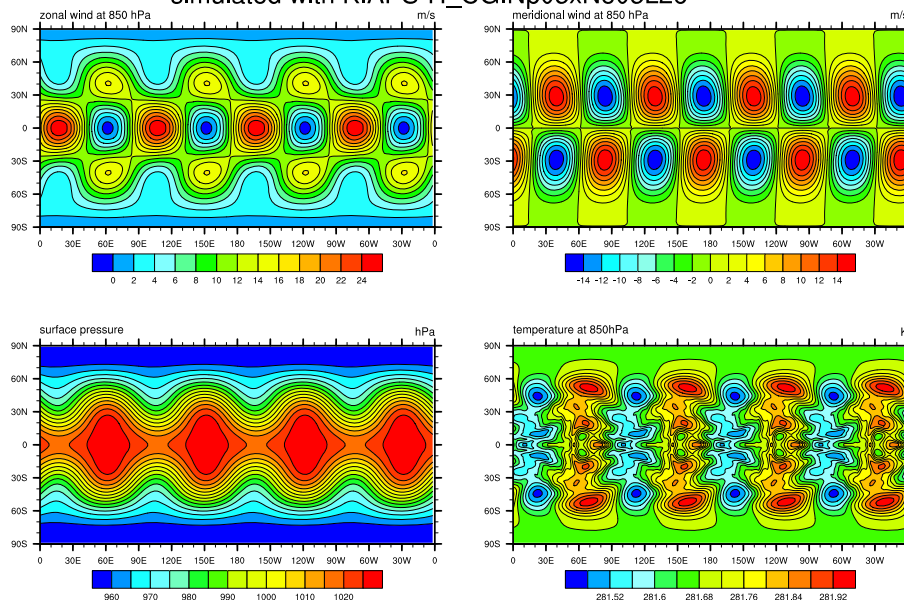


Figure 2. Numerical results for the CG simulation on the resolution of the $H = 64$ ($n_H = 8$ and $N = 8$) with 26 vertical levels: top row: 850 hPa zonal wind and meridional wind, bottom row: surface pressure and 850 hPa temperature.

Development of a hydrostatic dynamical core using the CG/DG methods

S.-J. Choi and
F. X. Giraldo

Title Page

Abstract

Introduction

Conclusions

References

Tables

Figures

◀

▶

◀

▶

Back

Close

Full Screen / Esc

Printer-friendly Version

Interactive Discussion

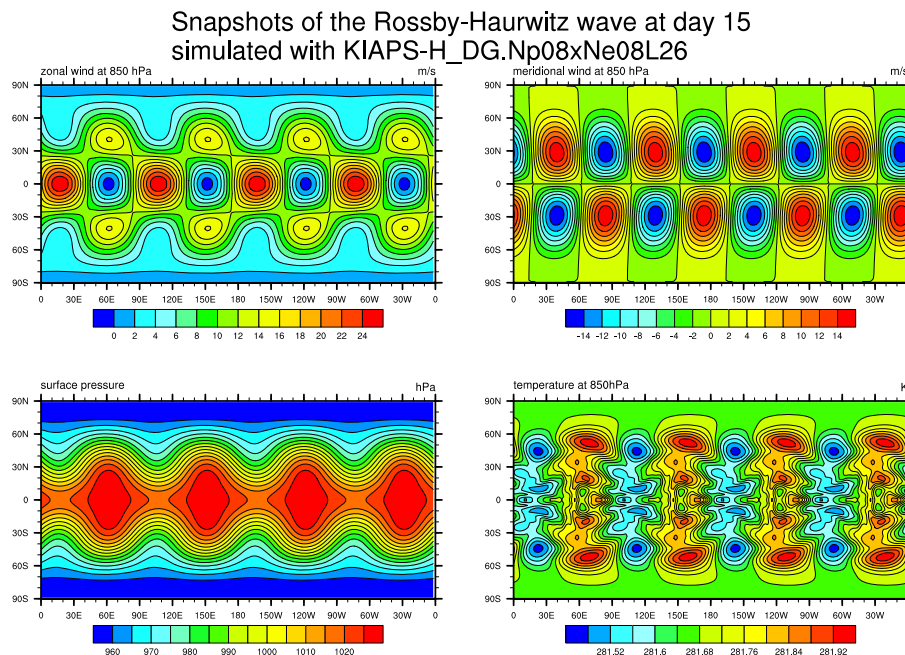


Figure 3. As in Fig. 2 but for the DG simulation.

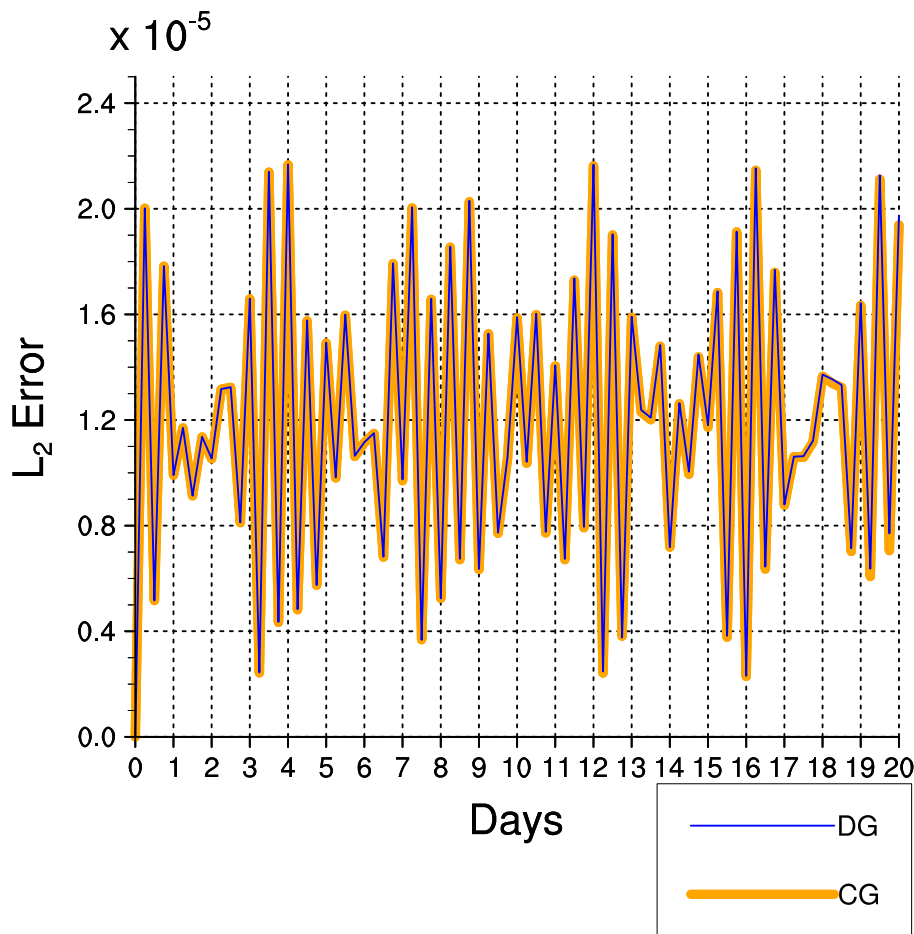


Figure 4. L_2 error norm of surface pressure in Pa for the CG and DG simulations at the $H = 128$ ($n_H = 16$ and $N = 8$) horizontal resolution and 26 vertical levels.

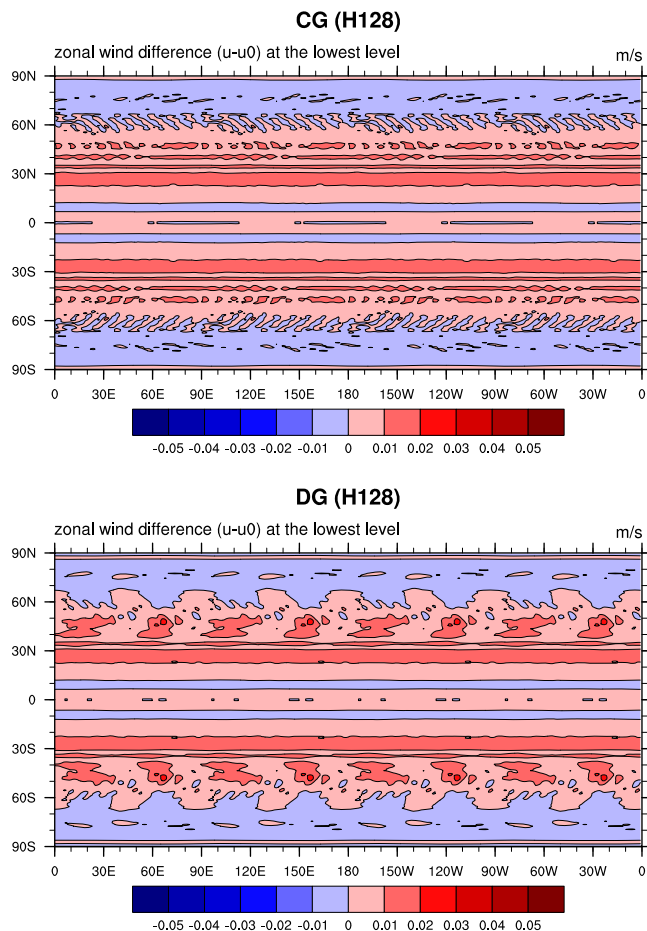


Figure 5. Distribution of zonal wind difference at the lowest model level between day 20 and day 0 for the (top) CG and (bottom) DG simulations at the $H = 128$ ($n_H = 16$ and $N = 8$) horizontal resolution and 26 vertical levels.

Development of a hydrostatic dynamical core using the CG/DG methods

S.-J. Choi and
F. X. Giraldo

Title Page

Abstract

Introduction

Conclusions

References

Tables

Figures

◀

▶

◀

▶

Back

Close

Full Screen / Esc

Printer-friendly Version

Interactive Discussion

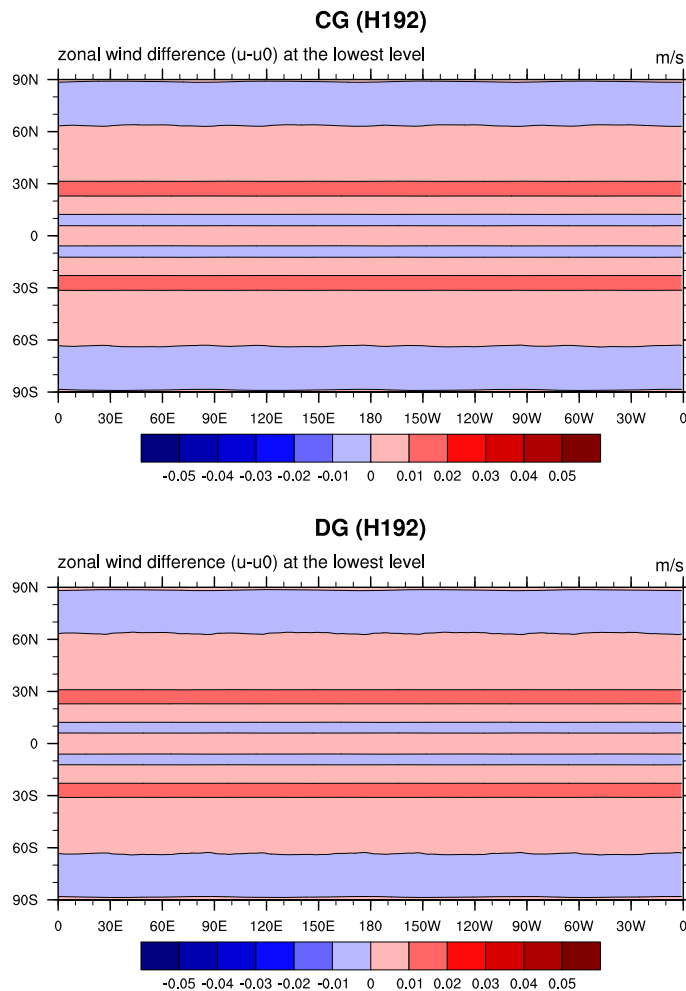


Figure 6. As in Fig. 5 but for the $H = 192$ ($n_H = 16$ and $N = 12$) horizontal resolution.

Development of a hydrostatic dynamical core using the CG/DG methods

S.-J. Choi and
F. X. Giraldo

Title Page

Abstract

Introduction

Conclusions

References

Tables

Figures

◀

▶

◀

▶

Back

Close

Full Screen / Esc

Printer-friendly Version

Interactive Discussion

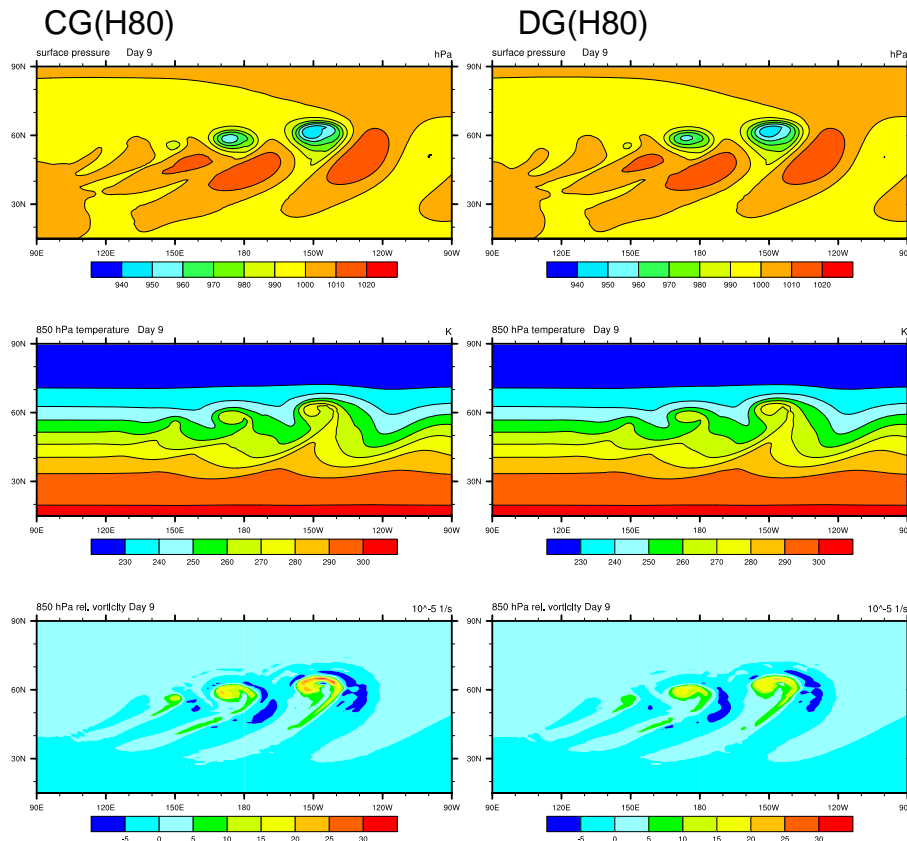


Figure 7. Baroclinic wave at day 9 with the (left) CG and (right) DG simulations with the resolution of the $H = 80$ ($n_H = 16$ and $N = 5$) horizontal resolution and 26 vertical levels: (upper row) surface pressure, (middle row) 850 hPa temperature, and (bottom row) 850 hPa relative vorticity at days (left) 7 and (right) 9.

Development of a hydrostatic dynamical core using the CG/DG methods

S.-J. Choi and
F. X. Giraldo

Title Page

Abstract

Introduction

Conclusions

References

Tables

Figures

◀

▶

◀

▶

Back

Close

Full Screen / Esc

Printer-friendly Version

Interactive Discussion

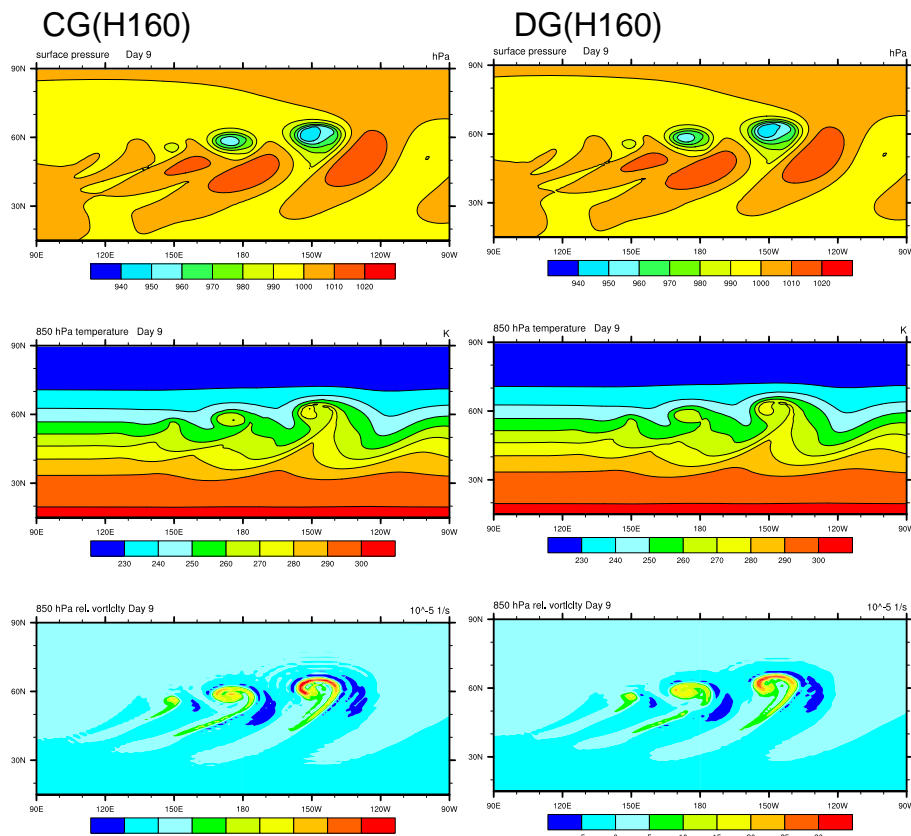


Figure 8. As in Fig. 7 but for the $H = 160$ ($n_H = 32$ and $N = 5$).

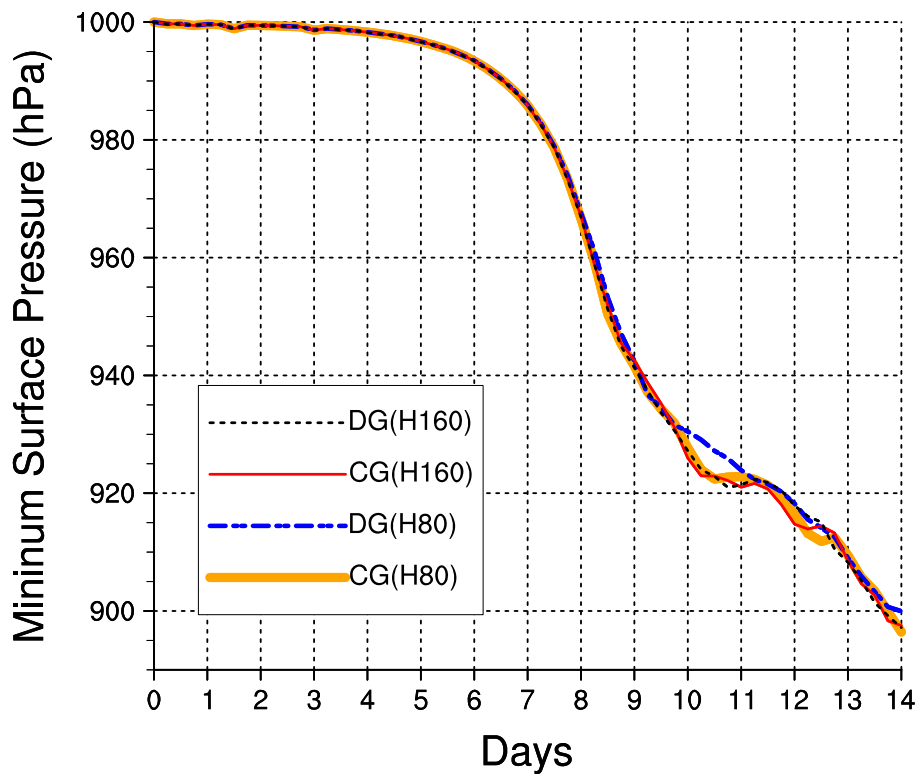


Figure 9. The minimum surface pressure (hPa) as a function of days for the CG and DG simulations with the lower resolution of the $H = 80$ ($n_H = 16$ and $N = 5$) and the higher resolution of the $H = 160$ ($n_H = 32$ and $N = 5$).

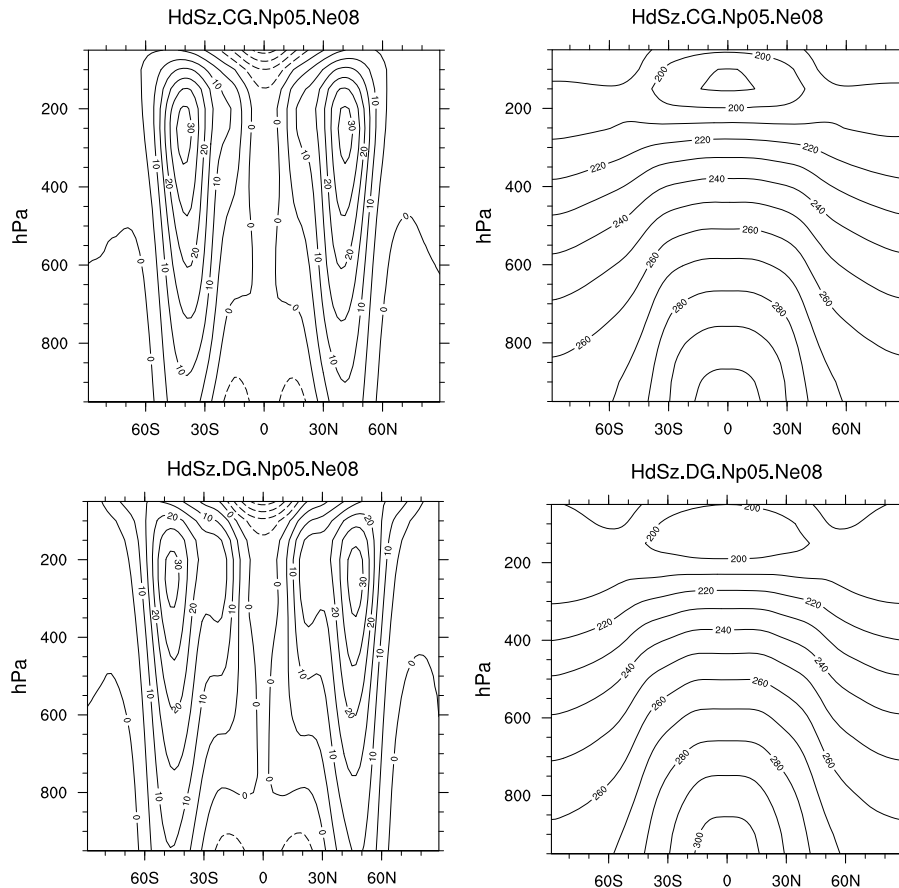


Figure 10. The (left) mean zonally averaged zonal velocity (m s^{-1}) and (right) mean zonally averaged temperature (K) for the (upper row) CG and (bottom row) DG simulations with the resolution of the $H = 40$ ($n_H = 8$ and $N = 5$) and 25 vertical levels ($N_{\text{lev}} = 25$). These are calculated over the last 1000 days of a 1200 day integration.

Development of a hydrostatic dynamical core using the CG/DG methods

S.-J. Choi and
F. X. Giraldo

Title Page

Abstract

Introduction

Conclusions

References

Tables

Figures

◀

▶

◀

▶

Back

Close

Full Screen / Esc

Printer-friendly Version

Interactive Discussion

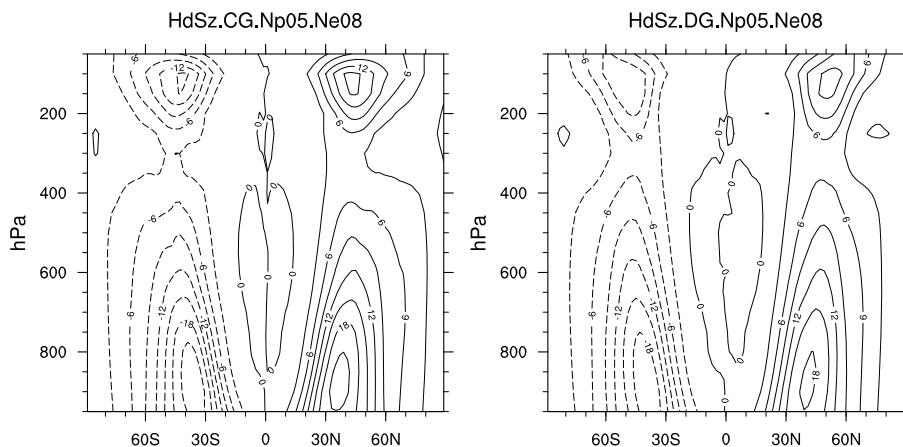


Figure 11. The mean zonally averaged eddy heat flux for the (left) CG and (right) DG simulation with the resolution of the $H = 40$ ($n_H = 8$ and $N = 5$).